Los Alamos National Laboratory is operated by the University of California for the United States Department of Energy under contract W-7405-ENG-36.

The Use of Optical Fibers for Shock Pressure and Timing Measurements at High Pressures

Los Alamos
Los Alamos National Laboratory
Los Alamos, New Mexico 87545

Prepared by Janis M. Gibbs, Group M-4

LA-11148-MS

UC-37
Issued: January 1988

The Use of Optical Fibers for Shock Pressure and Timing Measurements at High Pressures

Michael J. George
Ralph Menikoff
Lynn R. Veeser

Los Alamos National Laboratory
Los Alamos, New Mexico 87545

THE USE OF OPTICAL FIBERS FOR SHOCK PRESSURE AND TIMING MEASUREMENTS AT HIGH PRESSURES

by

Michael J. George, Ralph Menikoff, and Lynn R. Veeser

ABSTRACT

We have investigated the use of quartz fibers as arrival-time detectors and as absolute pressure transducers for shock waves at pressures of 50 GPa and higher. Four experiments were fired in which a steel flyer plate impacted an instrumented steel target plate. Arrival times measured with the fibers are compared with those given by more conventional electrical pin switches. Additional signal features are related to hydrodynamic events and compared with calculations. Calibrated signal voltages are related to shock temperatures through blackbody radiation theory. The temperatures are then related to pressures using shock Hugoniot data, and the results compare favorably with those of the hydrodynamic calculations.

I. INTRODUCTION

Electrical pins and foil switches work reliably at shock pressures of 100 GPa (1 Mbar) and higher. They are also sensitive to weak precursor shocks with strengths as low as 1 GPa. To detect the arrival of very high pressure shock waves without being pre-empted by possible low-pressure disturbances, we need a detector with an appropriately high threshold. We have investigated the use of optical fibers for this purpose. When a high-pressure shock wave enters a fiber from the surrounding medium, a hot, light-emitting shock front will be produced within the fiber itself. The amount of light that travels down the fiber will be determined largely by geometrical considerations. A high shock temperature is needed in the fiber to generate a detectable signal. Thus, we can have a fiber-optic "pin" that has a high pressure threshold. Furthermore, if we understand how the temperature in the fiber can be related to the pressure in the surrounding medium, the fiber has the possibility of becoming a continuous pressure transducer as the shock propagates along its length. A series of four experiments, M-4 Shots H-654, H-655, H-664, and

H-665, was conducted to test these principles. Hereafter these shots will be called the first through fourth experiments, respectively.

II. EXPERIMENTAL ARRANGEMENT

The basic experiment was to explosively drive a thin steel plate into a similar stationary plate at a slight angle, producing a phased collision. The physical arrangement is shown in Fig. 1. The explosive was estimated to accelerate the first plate up to 5 km/s, which would then produce a collision phase velocity of about 40 km/s. The layer of epoxy on the top surface of the target plate served to protect the instrumentation and to act as a hydrodynamic cushion.

The target plate was instrumented with four kinds of sensors at each of ten stations: 1) Cu-on-Kapton electrical foil switches, 2) Al-on-Mylar electrical foil switches, 3) optical fibers lying on the surface of the steel with egress to the right along with the electrical leads ("surface fibers"), and 4) optical fibers through small holes in the target plate with egress to the bottom through epoxy potting ("through fibers"). The electrical foil switches, hereafter called Cu and Al pins, were tested in two similar M-4 experiments, Shots H-164 and H-165, which were reported in M-4-1851, July 15, 1983.

III. FIBERS, FILTERS, AND DETECTORS

In the first two shots we tested two kinds of optical fibers, Raychem VSC-Al-1X-17, and Polymicro Technology FHP-100-110-135. Each is a radiation insensitive (low-impurity), 100-μm-diam core fiber commonly used by P Division for experiments in high-radiation environments. Since we saw little or no difference in the amount of light, we used only the Polymicro fiber, the easier one to handle, on the third and fourth tests.

The Polymicro fiber has a pure fused silica core with a thin, doped-glass cladding and a 135-μm-diam plastic jacket that is not nearly as fragile as it appears. We instrumented the shots with 2-m-long pieces having an OFTI connector on one end. Running from the experiment into the bunker to the detectors were 15-m cables (8 fibers each) that we protected and reused.

The optical detectors were model 902 APD receivers built by P-14. They are based on an RCA model C30948 silicon avalanche photodiode with a fast amplifier following. The sensitivity is 1.1×10^4 V/W, the bandwidth is about

Shots H-654, 655, 664 & 665

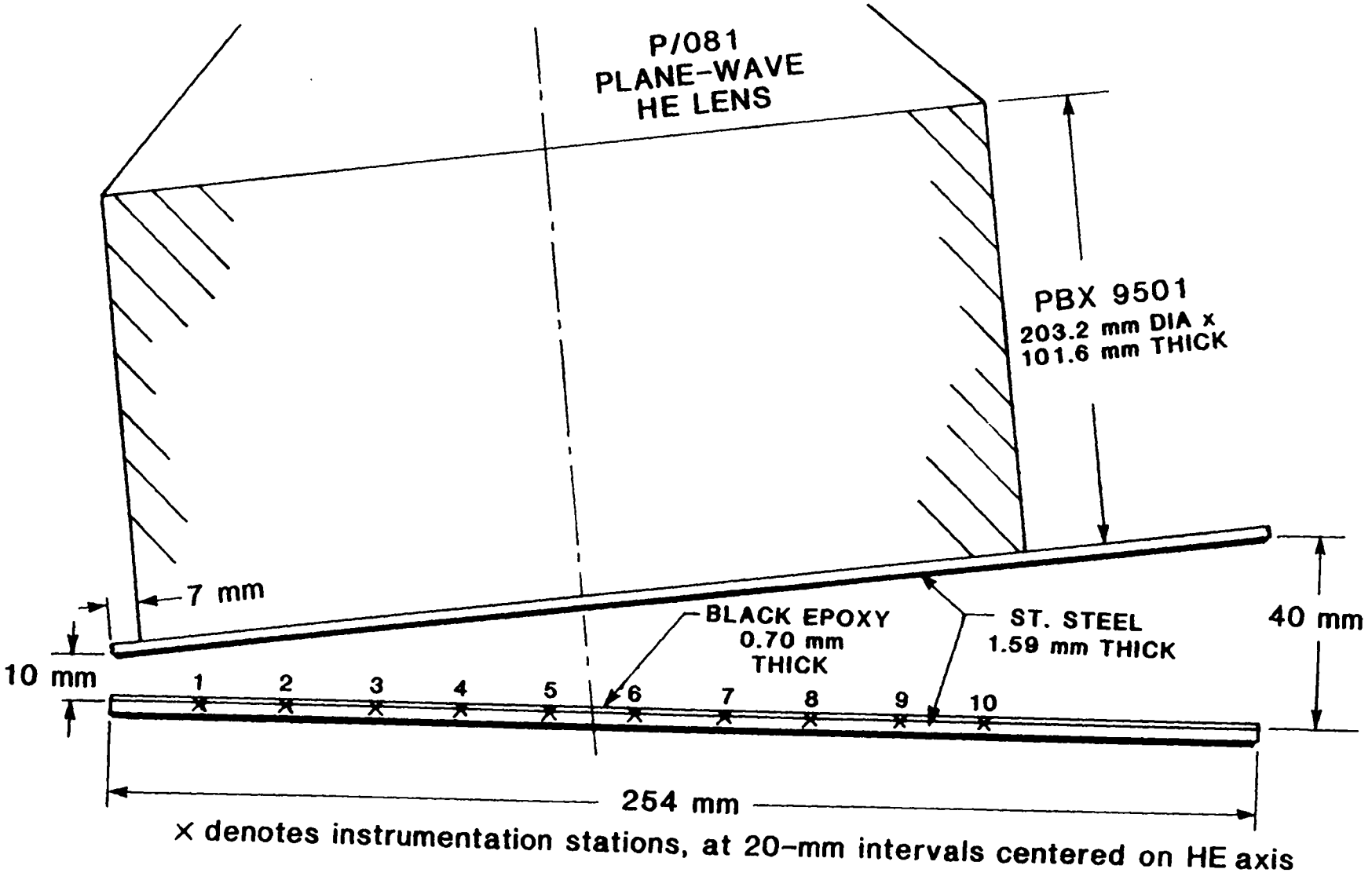

Fig. 1. Physical arrangement for all four experiments.

450 MHz, noise levels are <1 mV, and the maximum linear response occurs around 1 V output (100 μW, input). To help achieve high bandwidth, the receivers have been AC coupled, and the resulting drop in signal for a constant input is about 10%/μs. The spectral response drops off rapidly for wavelengths longer than 1000 to 1100 nm, and we filtered the inputs with Wratten 89B filters to absorb wavelengths shorter than 700 nm to reduce background light and help in the calibrations. For the fourth shot we added neutral density filters to reduce the signals by factors of 2 for the surface fibers and 7 for the through fibers.

For the first two shots, when we were unsure of the signals to expect, we followed the optical receivers with a 100-gain fast amplifier to be sure we would see some signal and to let us look carefully for any prepulses. We also removed all filters for these two shots.

The electrical signals from the optical receivers (or amplifiers) were power-divided, and each signal was sent to two LeCroy TR8828 digitizers; one recorded at high sensitivity (2 mV/sample bit) and one at low sensitivity (20 mV/bit).

IV. ARRIVAL-TIME MEASUREMENTS

In the first experiment, the epoxy on the target plate was not blackened, and sufficient light was received from shocked air in front of the driven plate to drive the detector amplifiers into saturation. Fast-breaking pulses were observed only from the Cu and Al electrical pins, and the data from these are given in Fig. 2. Instrumentation positions 1 and 10 are not shown because they are subject to severe end effects from the driver system. The time zero here and in all following data is an arbitrary timing fiducial, which occurs approximately 30 μs after the load-ring pulse that fires the detonators, and which appears on all of the TR8828 records. To within ones ability to read the plot, one cannot tell the difference between the two sets of data.

The epoxy was blackened for the second experiment, and this eliminated the early signals on the surface fibers so that fast-rising pulses were obtained. However, the pulses were still sufficiently large to drive the amplifiers well into saturation. The late through fibers still had slow precursors, which were now attributed to light from shocked air on the back side of the target plate. (The epoxy potting on the back side was blackened

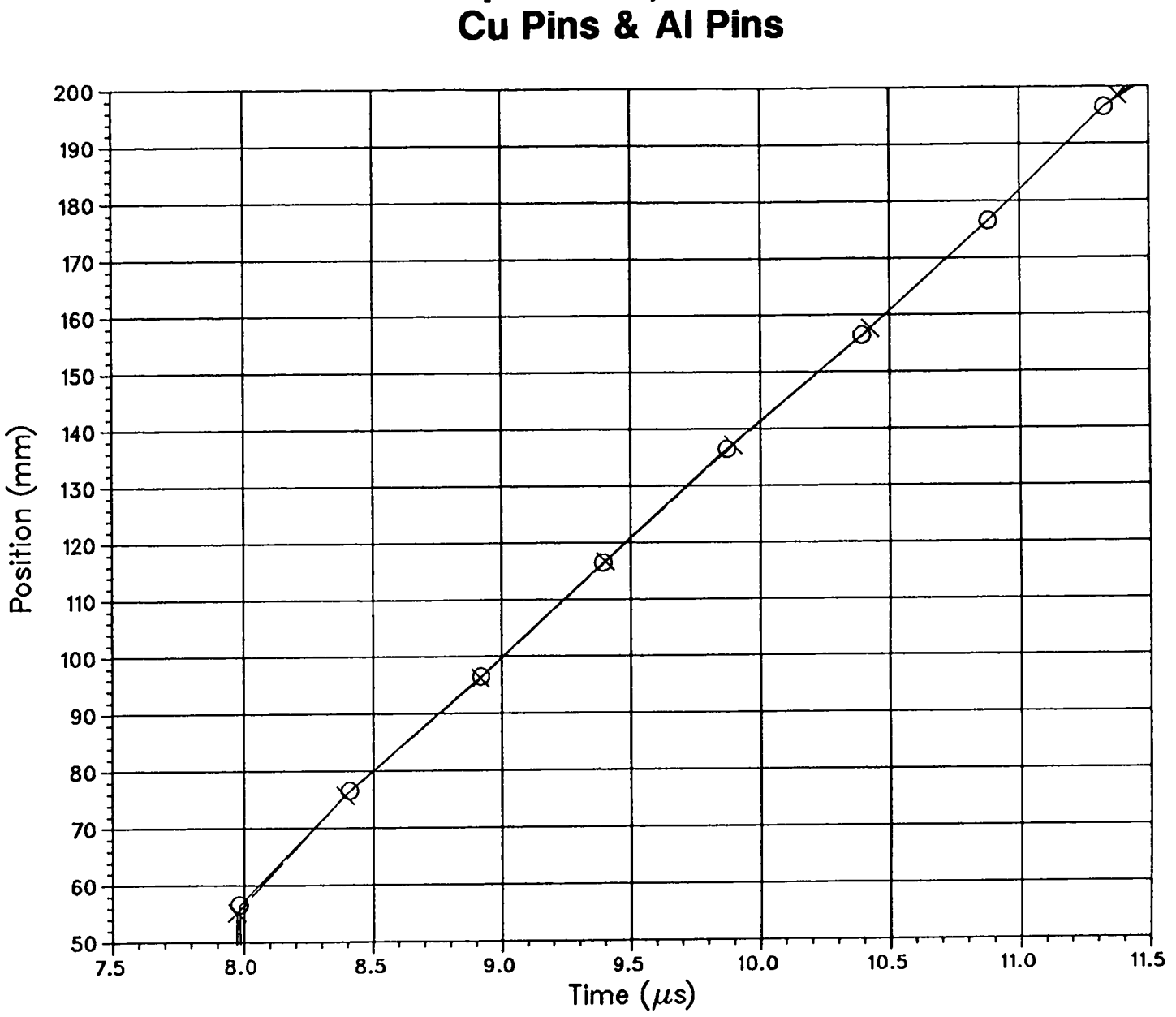

Fig. 2. Distance, from edge of plate, vs measured time for the first experiment. Only the central eight instrumentation positions are shown. Data are from Cu and Al wire pins only.

for the third and fourth experiments.) Fast-rising breaks were also found on the through-fiber pulses, corresponding to the times for the associated instrumentation stations. Therefore, good timing data were obtained on all four sets of sensors, and there was no evidence of any prepulse from a low-pressure shock in the epoxy, but the amplitude data were not interpretable because of the saturation. Figures 3-5 show various combinations of the data. In these plots and all others that follow in this format, the following symbol definitions are used consistently: Circle = Cu pins, X = Al pins, Triangle = surface fibers, and + = through fibers.

In the third experiment the amplifiers were left out, and the visible light (89B) filters were inserted. The signals were now well within the recording range, but some of the detectors were driven into the nonlinear output range. All of the signals now started with a sharp break from the baseline. However, several fibers were broken during the firing setup, probably because a severe snowstorm caused us to lose some of our patience and coordination. Figure 6 shows the data from Stations 2-9. Aluminum pins were not included in the third and fourth experiments.

The neutral-density optical filters were inserted for the fourth experiment, and these allowed the recording of signals of nearly optimum amplitude. Good timing data were obtained from all three sets of sensors, and these results are presented in Figs. 7-8. Two of the surface fibers (Stations 4 and 7) had a section of smaller core diameter fused to the front end, and a second sharp rise occurred in the signal at the diameter transition. These time-position points are included in the data plots and appear to lie on the trajectory, so that the possibility of measuring two arrival times with a single fiber has been realized. About 180 ns after their initial signal rise, the through fibers show a sharp amplitude reduction, which is attributed to the shock breakout on the back side of the target plate. These times are also plotted in Fig. 8. In Fig. 9 we plot the time difference between the initial signal rise and its fall for each of the 10 stations as a function of position. These are direct interval measurements and have very good precision. The decrease in the transit time with position is because of the increase in flyer plate velocity with distance of run. This is compatible with the increasing signal strength in the surface fibers and one-dimensional hydrodynamic calculations described in Sections VI and VII.

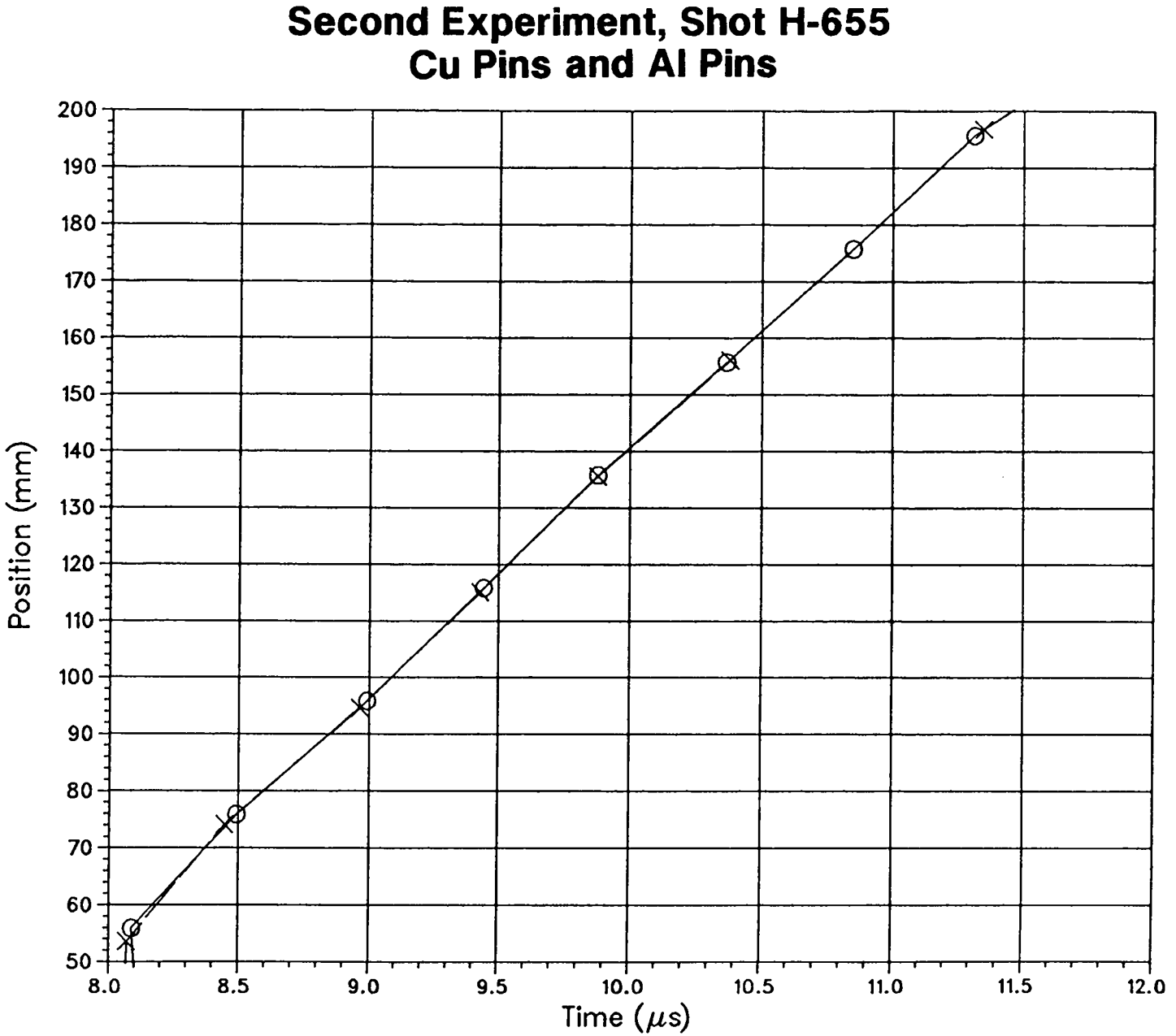

Fig. 3. Distance, from edge of plate, vs time for the second experiment, showing data from Cu and Al wire pins only.

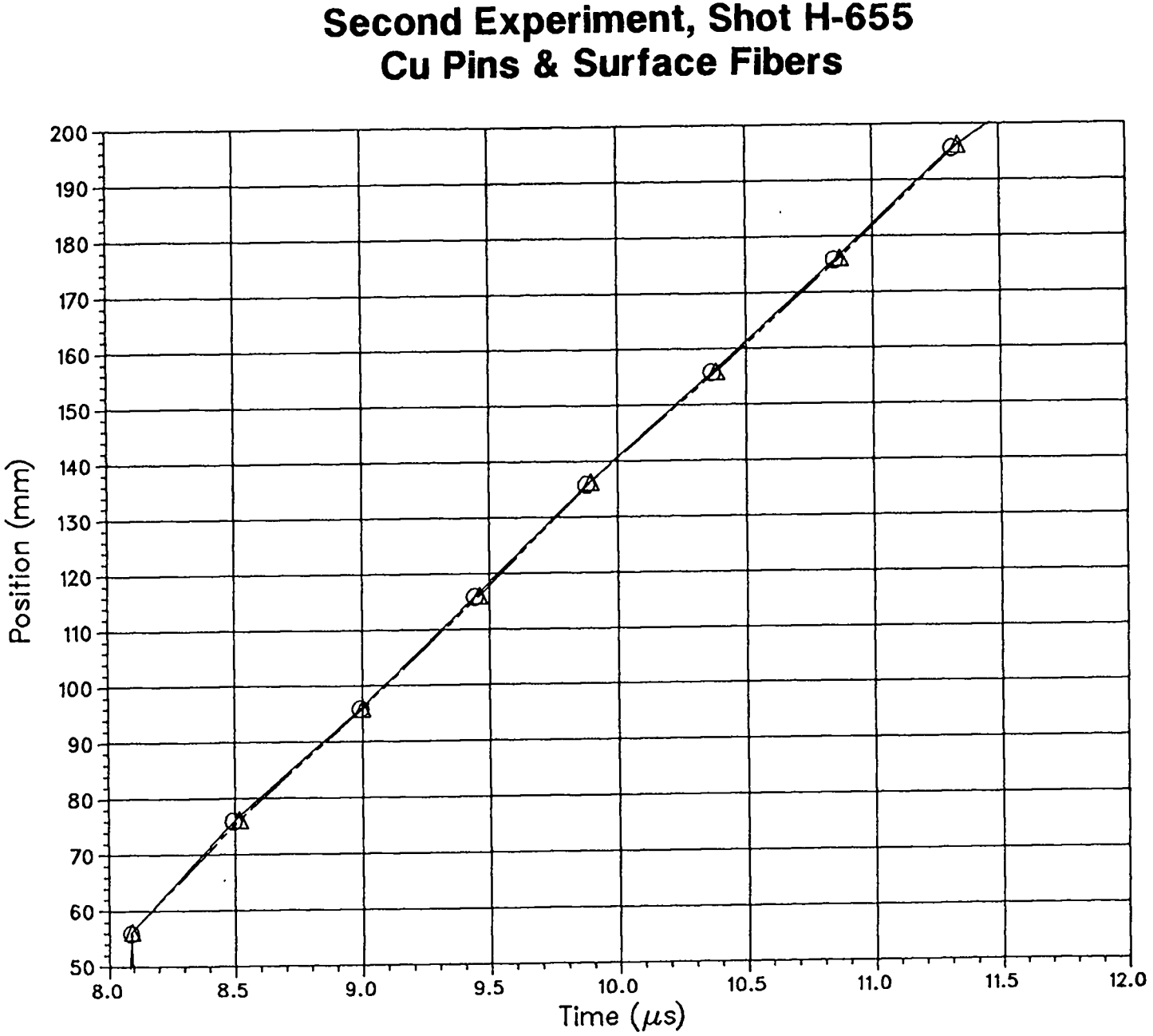

Fig. 4. Distance vs time for the second experiment, showing data from Cu wire pins and surface fibers.

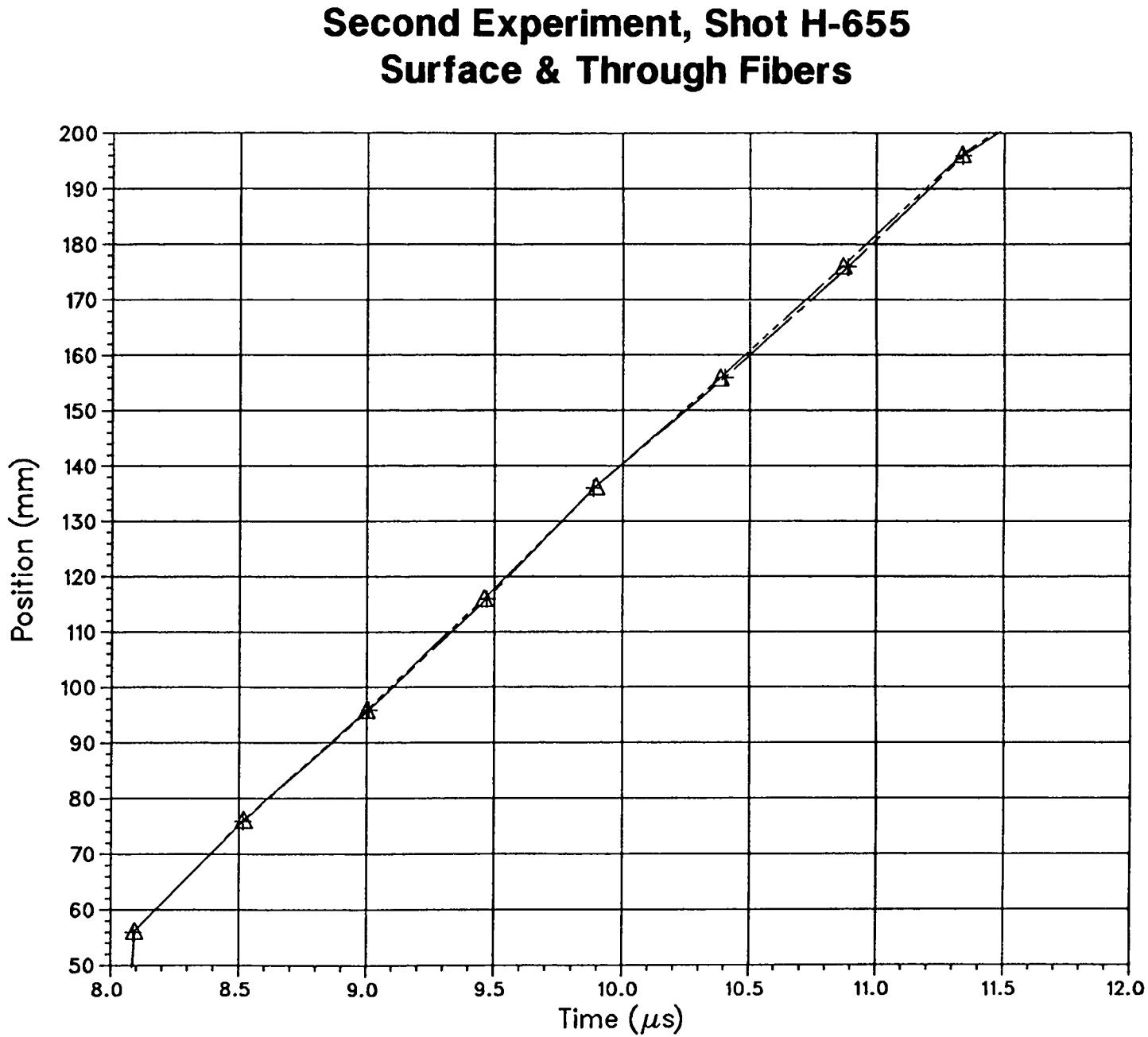

Fig. 5. Distance vs time for the second experiment, showing data from both groups of fibers.

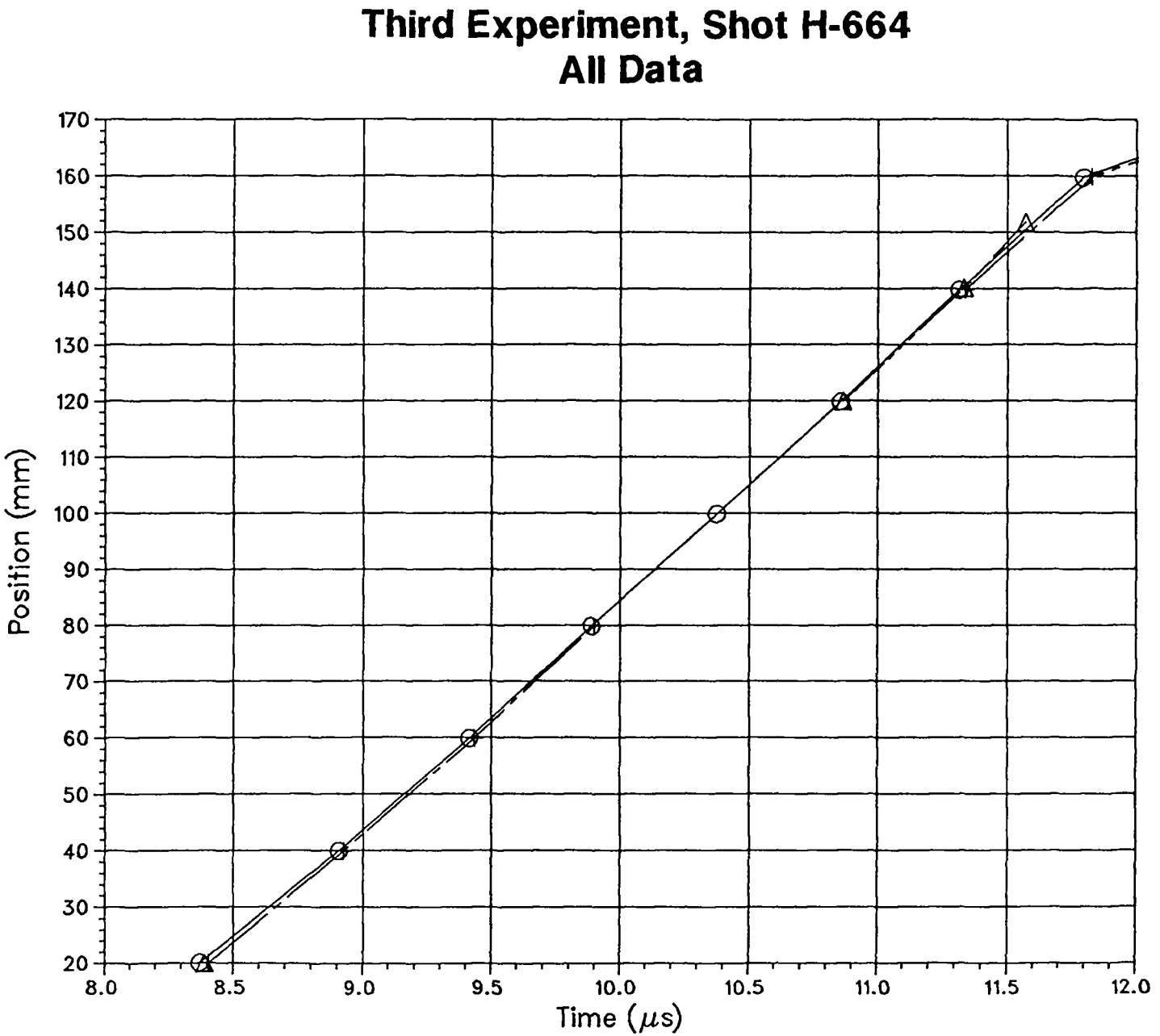

Fig. 6. Distance, from Station 1, vs time for the third experiment, showing data from Cu wire pins and all fibers, many of which were broken and gave no signals.

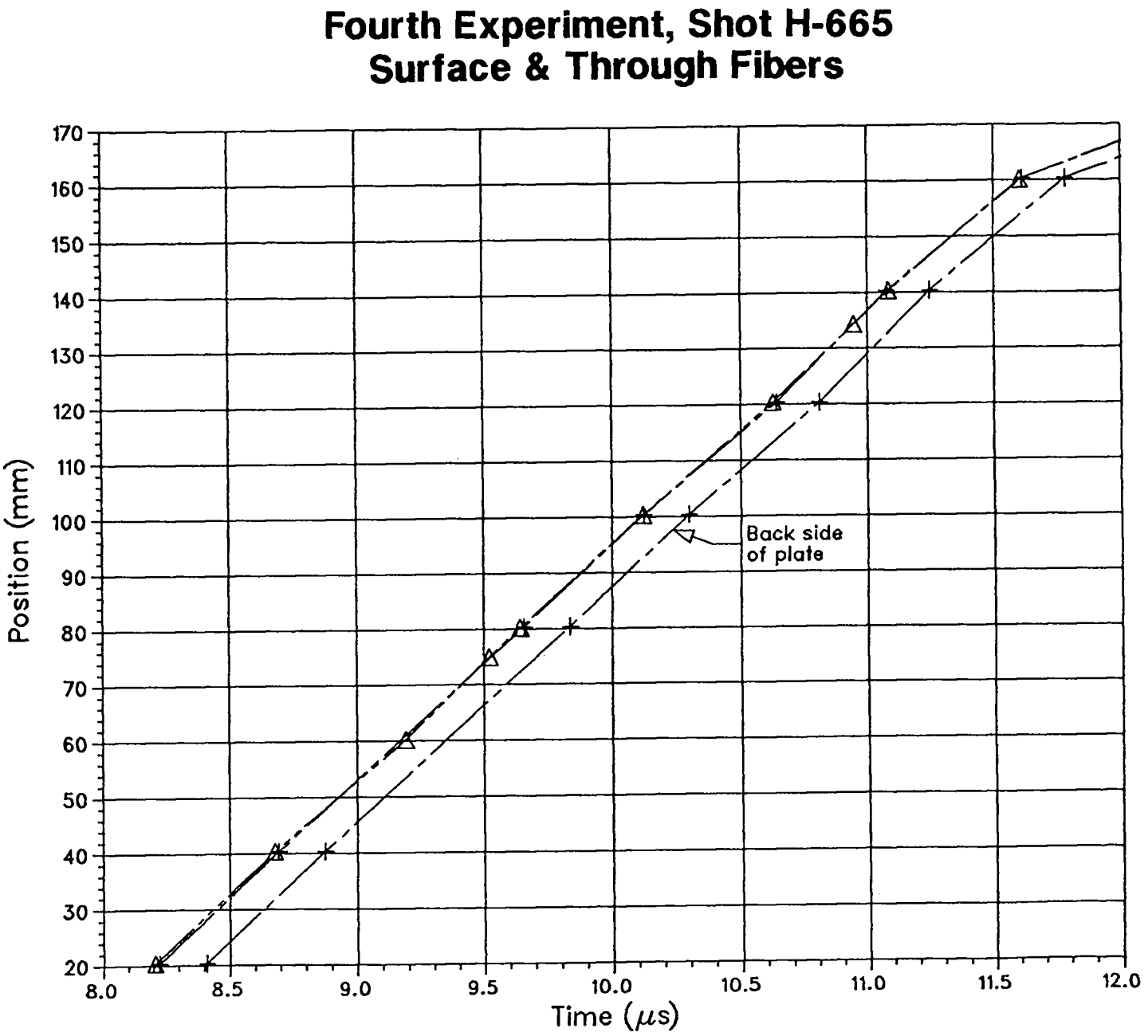

Fig. 8. Distance vs time for the fourth experiment, showing data from both groups of fibers, including breakout on the back side of the plate.

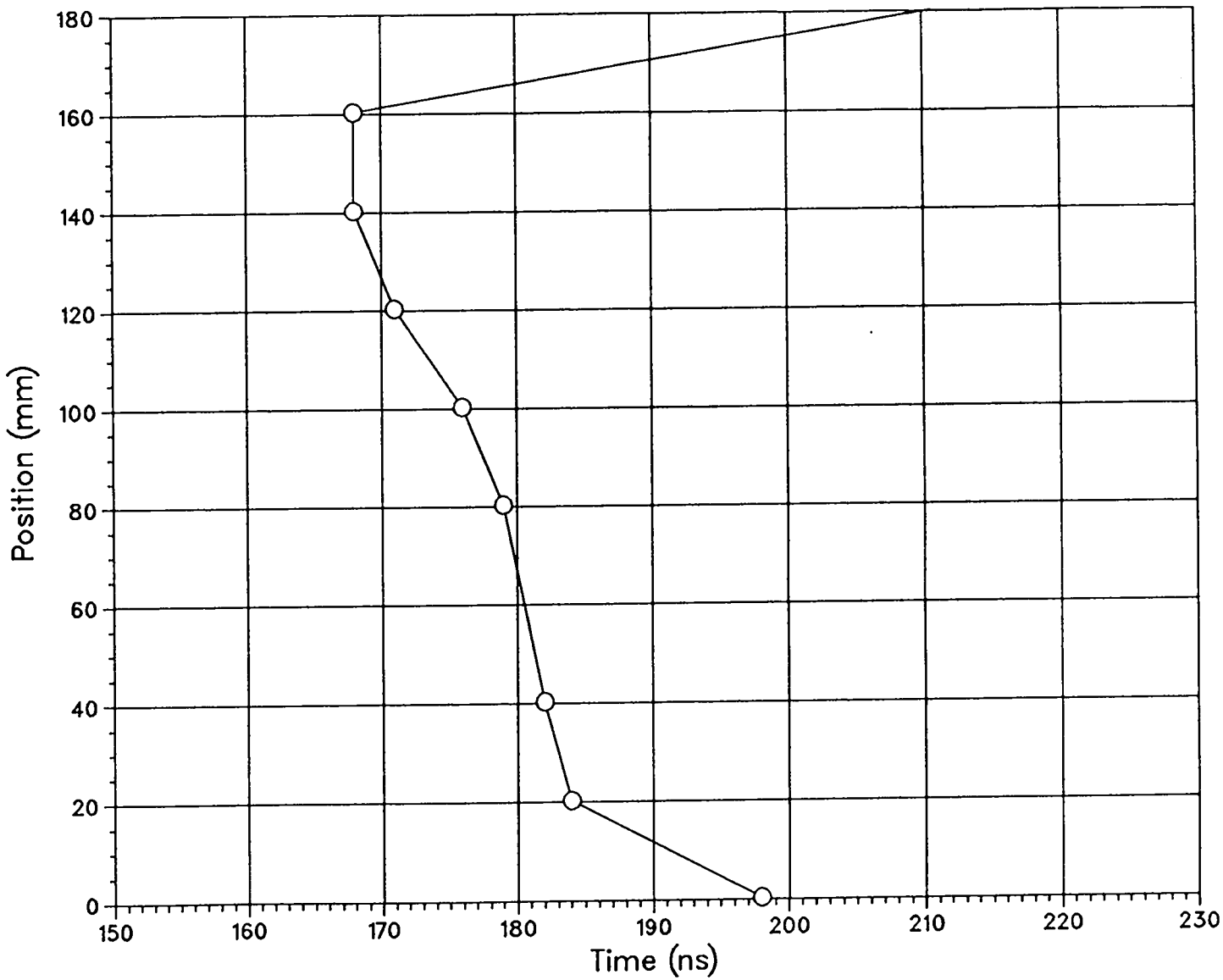

Fig. 9. Transit time through the steel plate, from initial pulse rise to sudden decrease, vs distance from Station 1.

The time differences between the various sets of sensors are so small that it is hard to read them from the data plots. The average differences from each experiment, using the Cu pins as a standard, are summarized in Table I. The surface fibers are later than the electrical pins, and the through fibers are later yet. The slightly increased delay in the later experiments may be related to the reduced recording sensitivity for the fibers.

V. SIGNAL AMPLITUDES AND SHOCK PRESSURES

To estimate the quartz fiber shock pressure from the amount of light produced, we begin by assuming that the end of the transparent fiber is in contact with a blackbody radiator (the shock-heated part of the fiber). For the convenience of the reader, some Planck radiation curves are plotted in Fig. 10. At wavelength λ, the blackbody at temperature T radiates an amount

$$L(\lambda) = \frac{2c^2h}{\lambda^5} \cdot \frac{1}{e^{hc/\lambda kT} - 1} \approx \frac{2.7 \times 10^{14}}{e^{To/T} - 1} \text{ W sr}^{-1} \text{ m}^{-3}$$

for $\lambda = 850$ nm and $To = 1.7 \times 10^{14}$ K. We estimate the solid angle of acceptance from the fiber numerical aperture, $NA = 0.25 \approx \sin\theta$, where θ is the half angle of the light that is totally internally reflected in the fiber core. Then the solid angle is $\Delta\Omega/4\pi = 0.016$. The area of the 100 μm diam core is $A = 7.8 \times 10^{-9}$ m^2, and the optical bandpass of the system is $\Delta\lambda \approx 300$ nm. Multiplying all these factors together gives the light power transmitted in one direction down the fiber,

$$P = L(\lambda)\, A\, \Delta\lambda\, \Delta\Omega/4\pi = \frac{1.0 \times 10^{-2}}{e^{To/T} - 1} \text{ W} \quad .$$

For a 60-GPa shock in the quartz, we expect a temperature of T = 3600 K and a power of $P = 90$ μW.

At these temperatures there is not enough light to measure the spectrum to verify the blackbody assumption. In an earlier experiment we measured the visible spectrum from a hotter ($\approx$2 eV) shock-heated fiber using a spectrometer and a streak camera; there was no evidence of spectral lines, but for that case we could not measure the entire spectral shape because most of the light is in the shorter wavelength region.

TABLE I

Average Time Delay from Cu Pins
(nanoseconds)

Experiment No.	Al Pins	Surface Fibers	Through Fibers
1	5	—	—
2	3	9	19
3	—	14	22
4	—	18	22

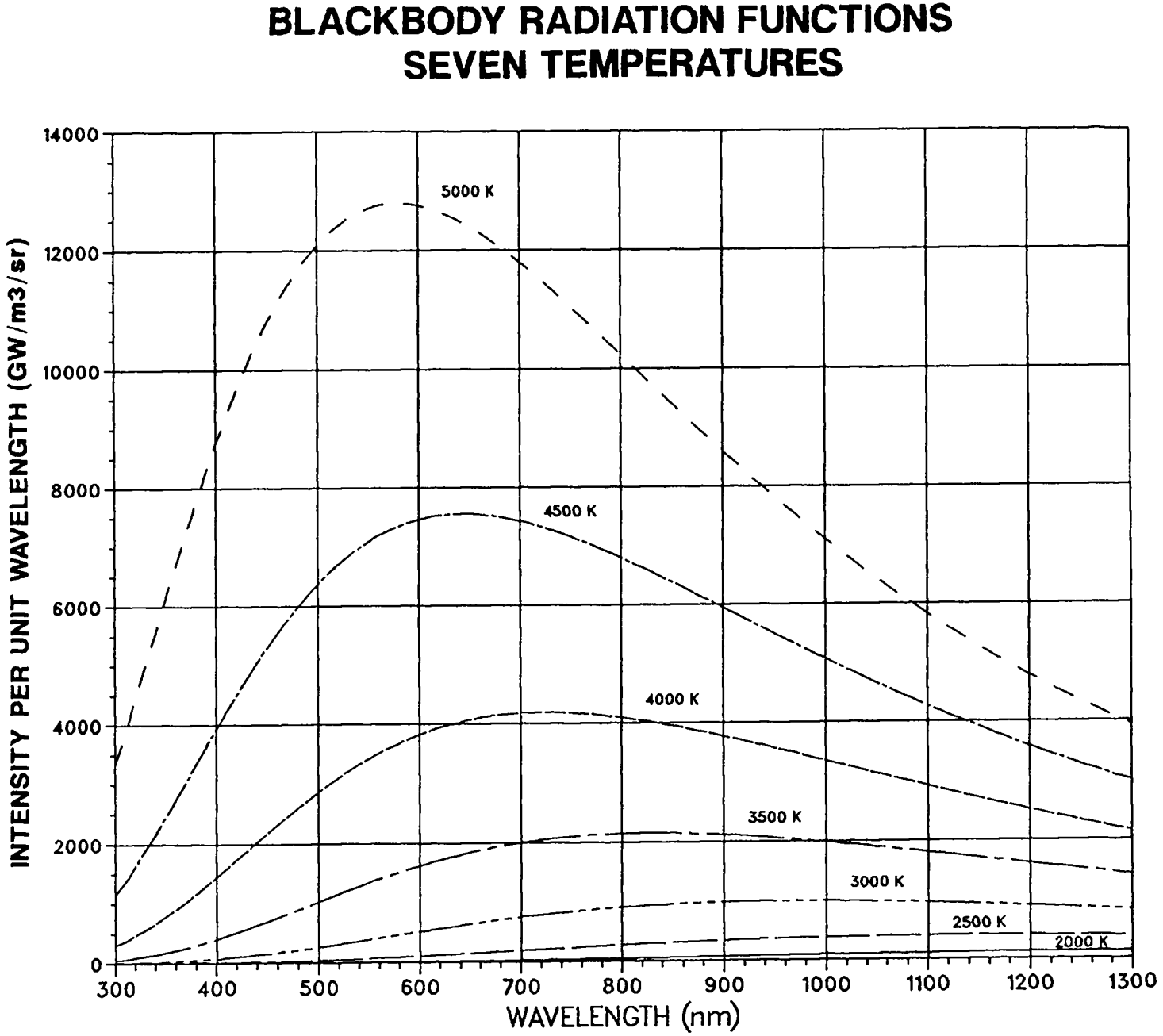

Fig. 10. Blackbody radiation intensity, power per unit area per steradian per unit wavelength, as a function of wavelength for selected temperatures.

Figure 11 shows the relationship between quartz pressure and temperature on the shock Hugoniot; it is taken from the Sesame equation-of-state tables. A least squares fit to the curve of Fig. 11 gives $T \approx -2000 + 97\ p - .044\ p^2$, where the temperature is in K and p is the pressure in GPa. Figure 12 gives the optical power from a fiber, again as a function of the shock pressure in the quartz.

We checked the transmission of the system by first inserting an 850-nm light source into the optical detector and then installing the filters and the 15-m cables and remeasuring the signals. Overall transmissions were 0.50 for the surface fibers and 0.14 for the through fibers for Shot 4, where we used different amounts of neutral-density filtering for the two cases. For Shot 3, where we used the same Wratten 89B filters but no neutral-density filters, transmissions were about 0.8. We estimate the transmission measurements to be accurate to about ±20%.

Presently we are trying to fabricate a light-emitting-diode-based calibration system that will overfill the fiber core to approximate the shot conditions and allow more accurate transmission measurements. That will be especially important when we need to use fiber-optic splitters, where the splitting ratio can depend on the mode structure of the light in the fiber core.

We calibrated the gain of the detectors using a stabilized light-emitting diode, the output of which was measured with a Tektronix 7F10 receiver. We also checked the gain of the 7F10 and found it to be accurate. The gain calibrations are estimated to be accurate to about ±10%. All the gains were set to 11 mV/μW.

Figures 13-14 show results from two surface fibers and two through fibers on Shot 4, both pairs from Stations 3 and 5. A supplementary scale on the right-hand side gives the conversion to fiber-optic output powers for the surface fibers. The light-producing mechanism for the through fibers is thought to be more complex and less well understood; therefore, we have not included a similar scale for that measurement.

The surface fiber from Station 1 gave a signal that increased gradually as the moving plate crushed the fiber. The signal was approximately constant from 10.0 to 11.7 μs, at which time it became very irregular. The other nine surface fibers all had sharp rises at later times, consistent with their positions on the plate, and then they agreed with the Station-1 signal quite

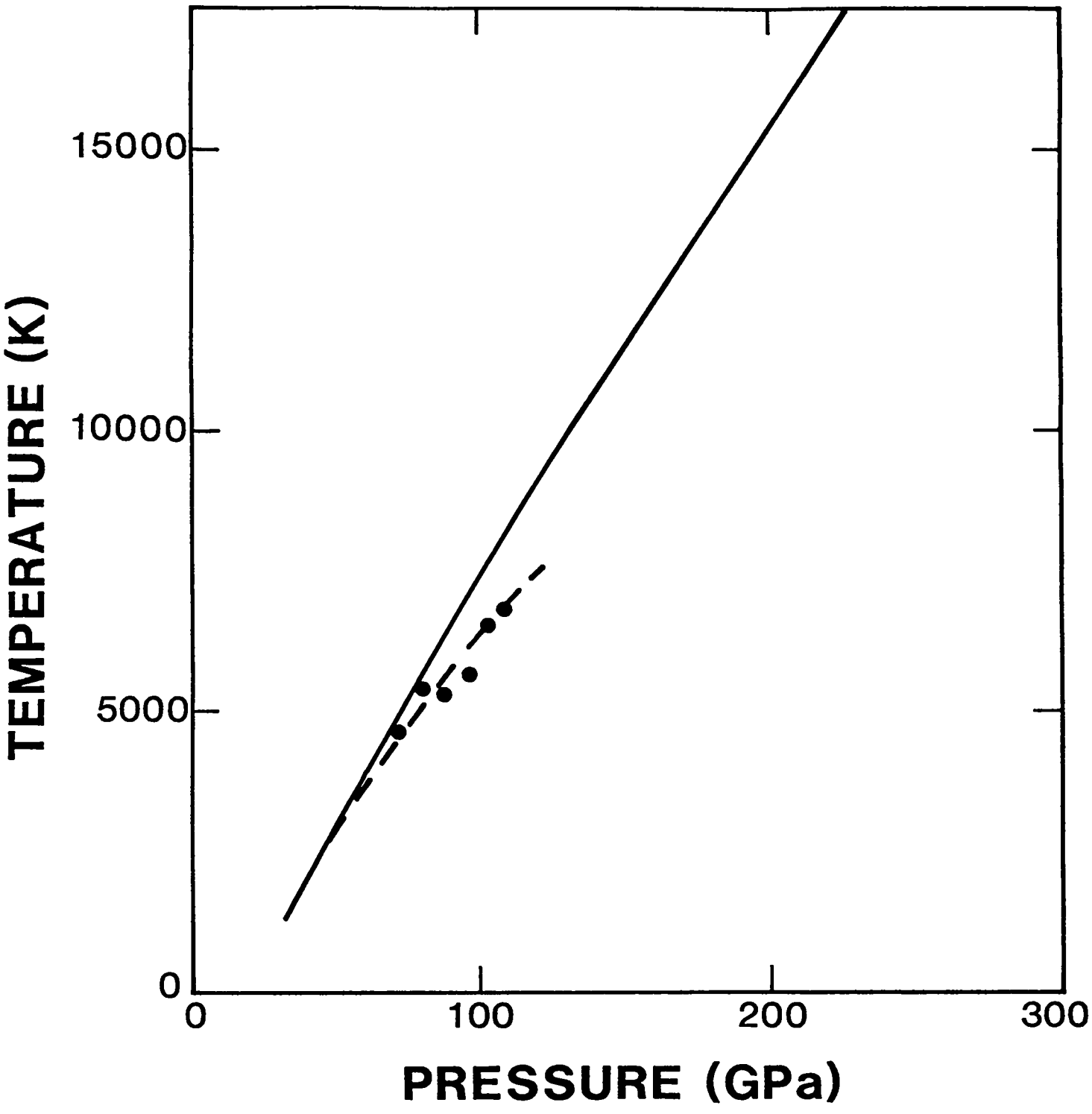

Fig. 11. Quartz temperature vs pressure for the shock Hugoniot. The curve is taken from the Sesame equation-of-state tables, and the points were measured by Lyzenga and Ahrens.[1]

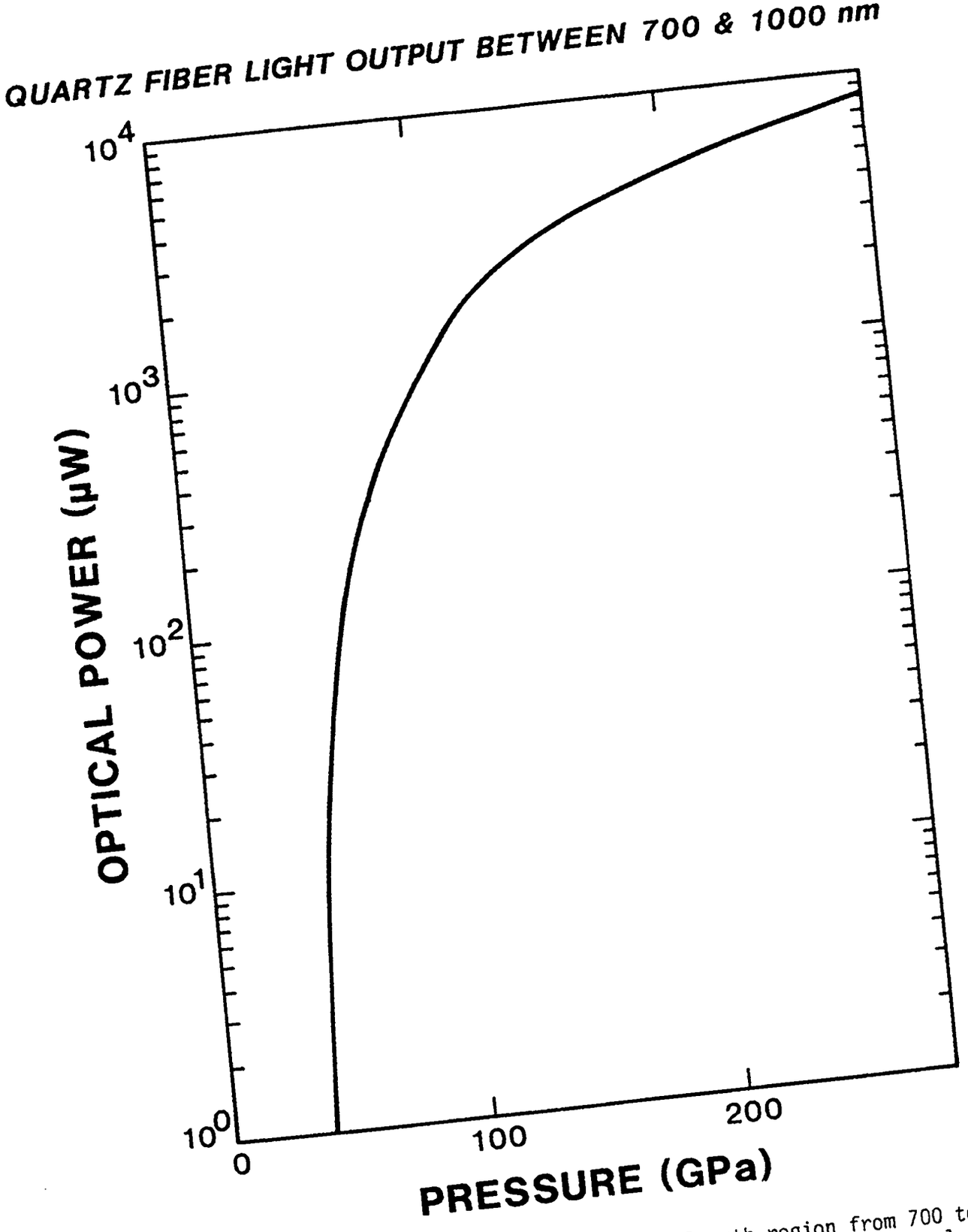

Fig. 12. Optical power emitted in the wavelength region from 700 to 1000 nm for a quartz fiber shock heated on its other end. The calculation assumes a 100-μm-diam fiber core, a numerical aperture of NA = 0.25, and no attenuation in the fiber.

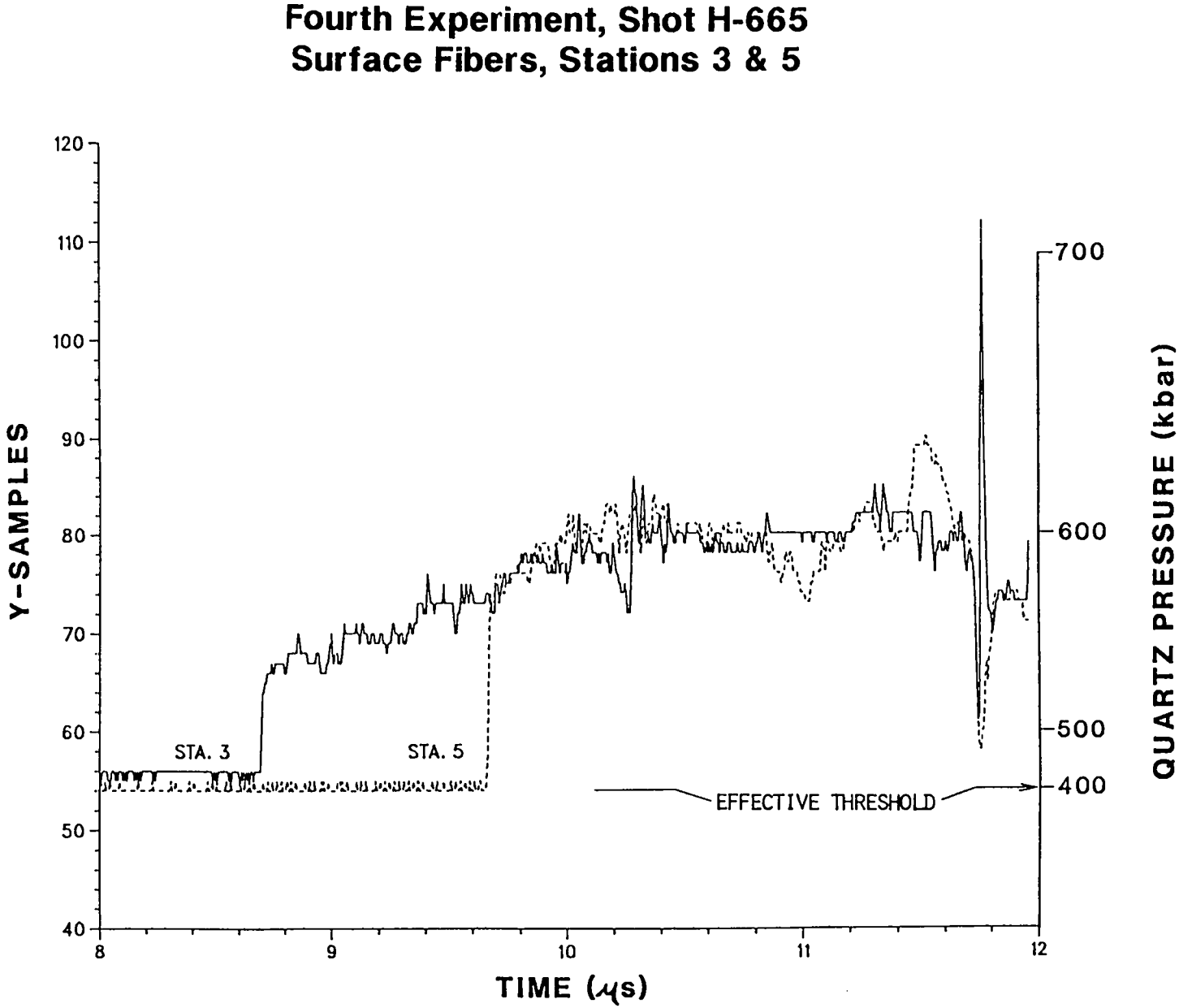

Fig. 13. Digitizer output data for the surface fibers at Stations 3 and 5 on Shot 4 with the conversion to fiber-optic output power.

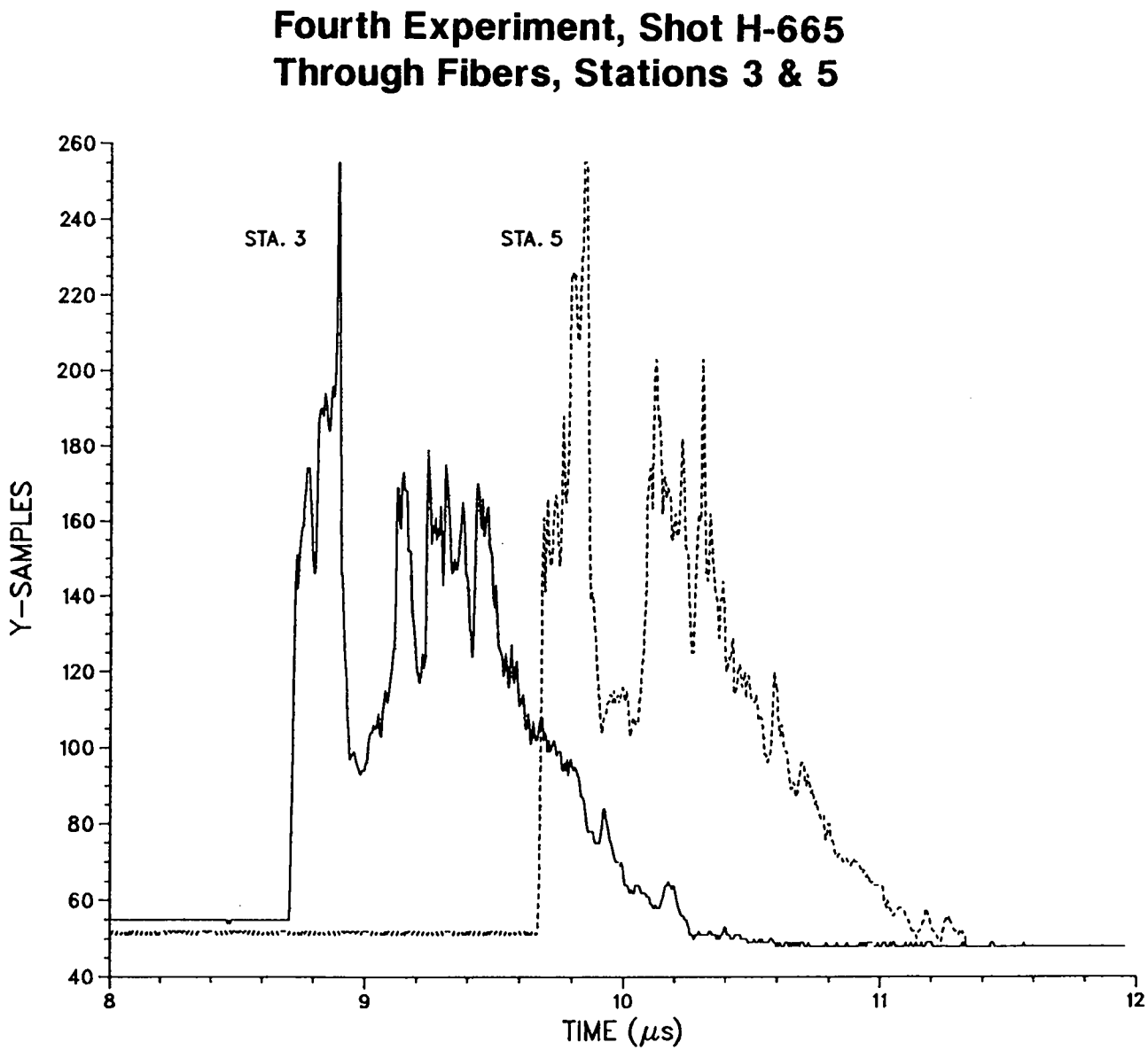

Fig. 14. Digitizer output data for the through fibers at Stations 3 and 5 on Shot 4.

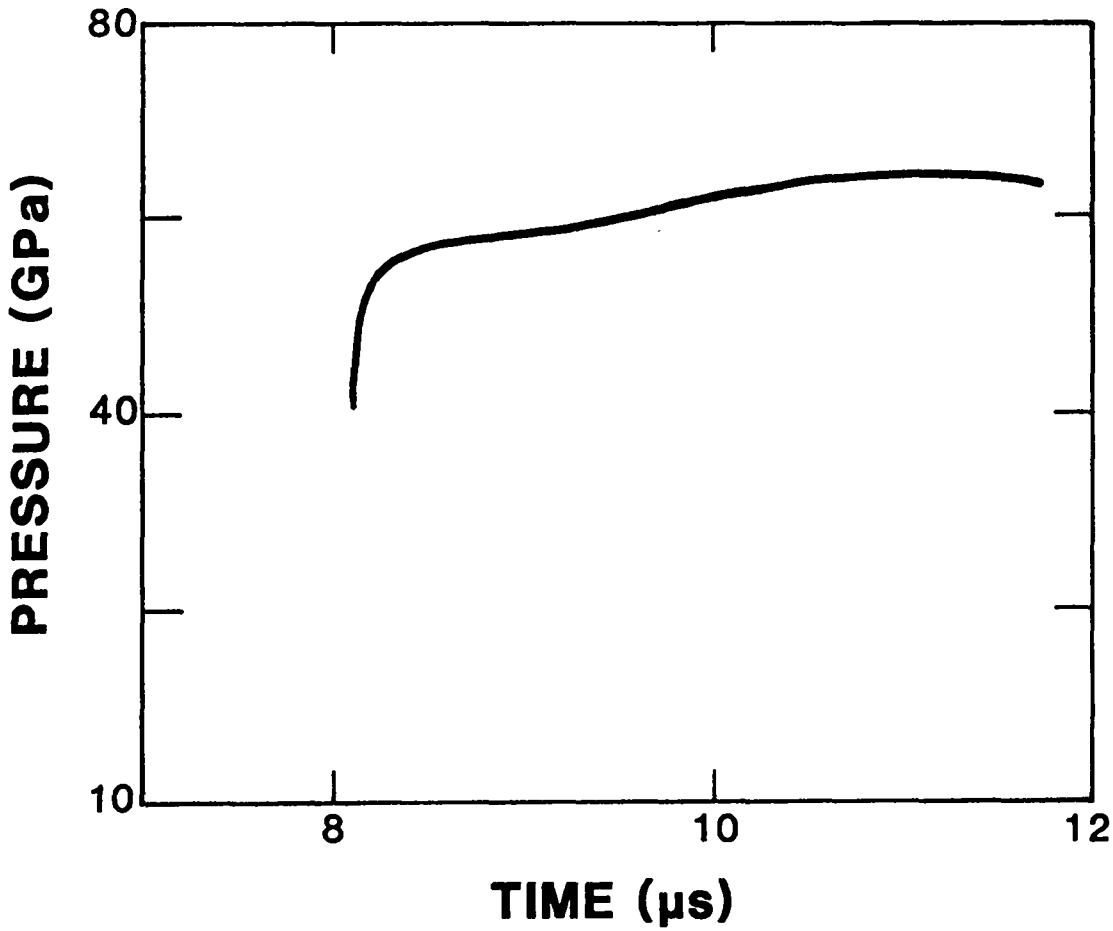

Fig. 15. Pressure vs time in the surface fibers as determined from the Station 1 surface fiber.

Fourth Experiment, Station 4.

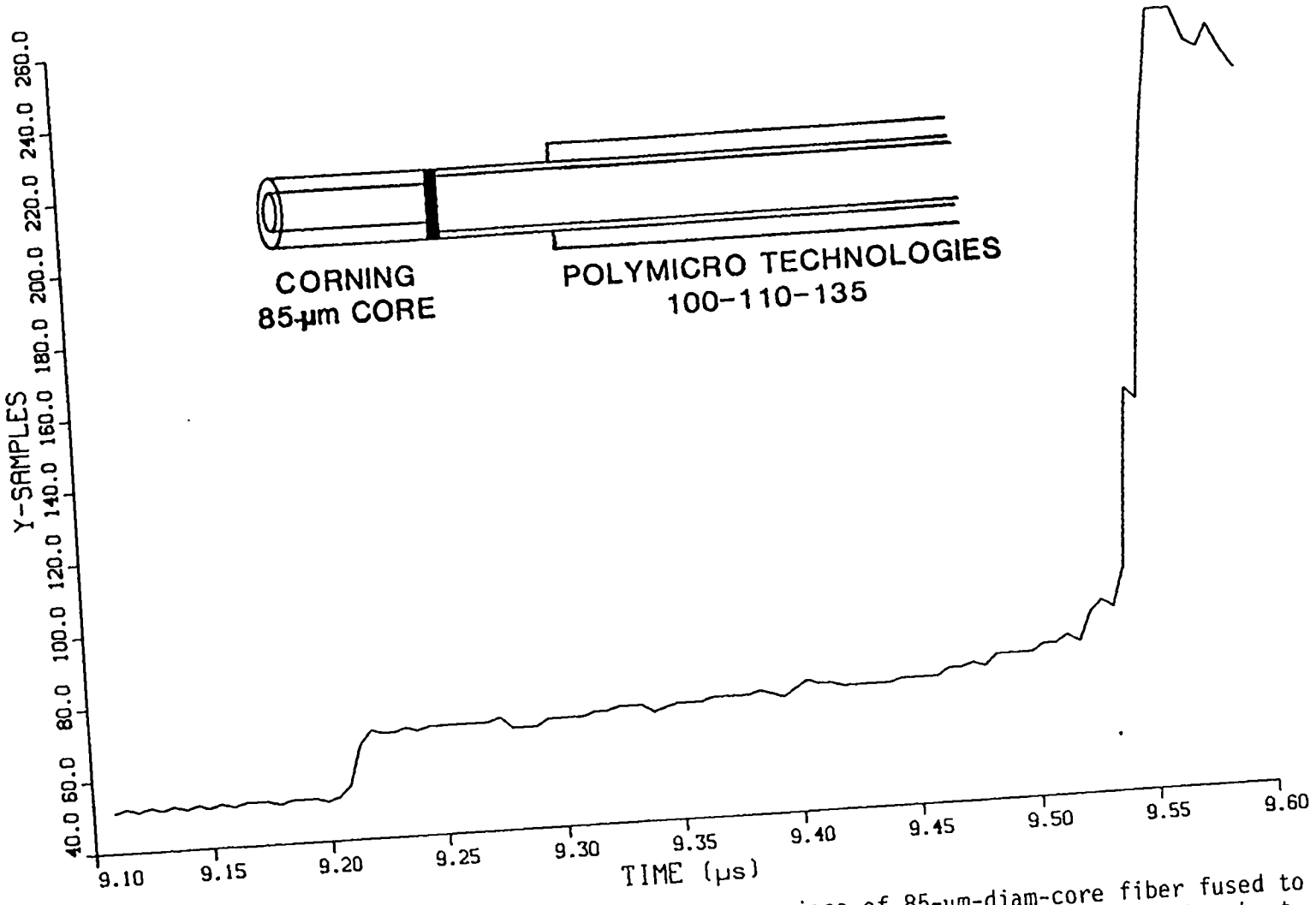

Fig. 16. Signal from a surface fiber with a 14.7-mm-long piece of 85-µm-diam-core fiber fused to its input end. The initial small rise in output is from the shock striking the end of the short piece, and the larger rise occurred when the main fiber was struck (trajectory data in Figs. 7 & 8).

than the main signal, perhaps because the weld did not transmit fully. There is also a small, gradual increase at the start of the second rise, probably indicating increased light coupling into the fiber when the shock nears the end of the narrow region. Nevertheless, we consider this test a success, as it shows the possibility of getting more than one time vs position measurement from a single fiber, although we will not be able to measure absolute light outputs and pressures from the fused-on piece.

VI. HYDRODYNAMIC CALCULATIONS

After the experiment, one-dimensional calculations with the HYDROX code[2] were used to obtain the velocity of the flyer plate and the pressure in the target. Figure 17 shows the velocity of the flyer plate as a function of distance of run. At Station 2, 15 mm of run, the velocity is 4.9 km/s, while at Station 9, 31 mm of run, the velocity has increased to 5.4 km/s. The flyer plate sends a weak shock into air, $p \approx 30$ MPa. The reflected air shock has a pressure $p = 380$ MPa, temperature $T = 13000$ K, and compression ratio $\rho/\rho_0 = 55$. The high temperature causes the air to radiate light and necessitates the optical fibers on the surface being coated or otherwise protected.

The air acts as a cushion between the flyer and the target. As the air is compressed, its pressure rises rapidly, and a shock is generated in the epoxy layer over the target plate with a pressure $p \approx 45$ GPa. This is approximately the pressure that would result from the impedance match between the flyer and epoxy neglecting the air. The shock in the epoxy reflects off the steel target with a pressure $p \approx 105$ GPa. A subsequent compression wave from a reflection in the epoxy catches up to the steel shock and strengthens it to a pressure $p \approx 170$ GPa. This is approximately the pressure that would result from the impedance match between the flyer and the steel target neglecting both the epoxy and air. The wave interactions can be seen from the pressure contours in the distance-time plane shown in Fig. 18. The pressure profiles in the flyer and target during their collision are shown in Fig. 19. For 20-mm distance of run of the flyer (approximately Station 4), the calculation predicts a transit time for the shock in the target of 200 ns, compared with the measured value of 180 ns seen in Fig. 9. Furthermore, the compression wave catches up and strengthens the shock in the target after approximately 95 ns, which is presumed to be the cause of a second signal increase observed on most of the through fibers. The measured times for this

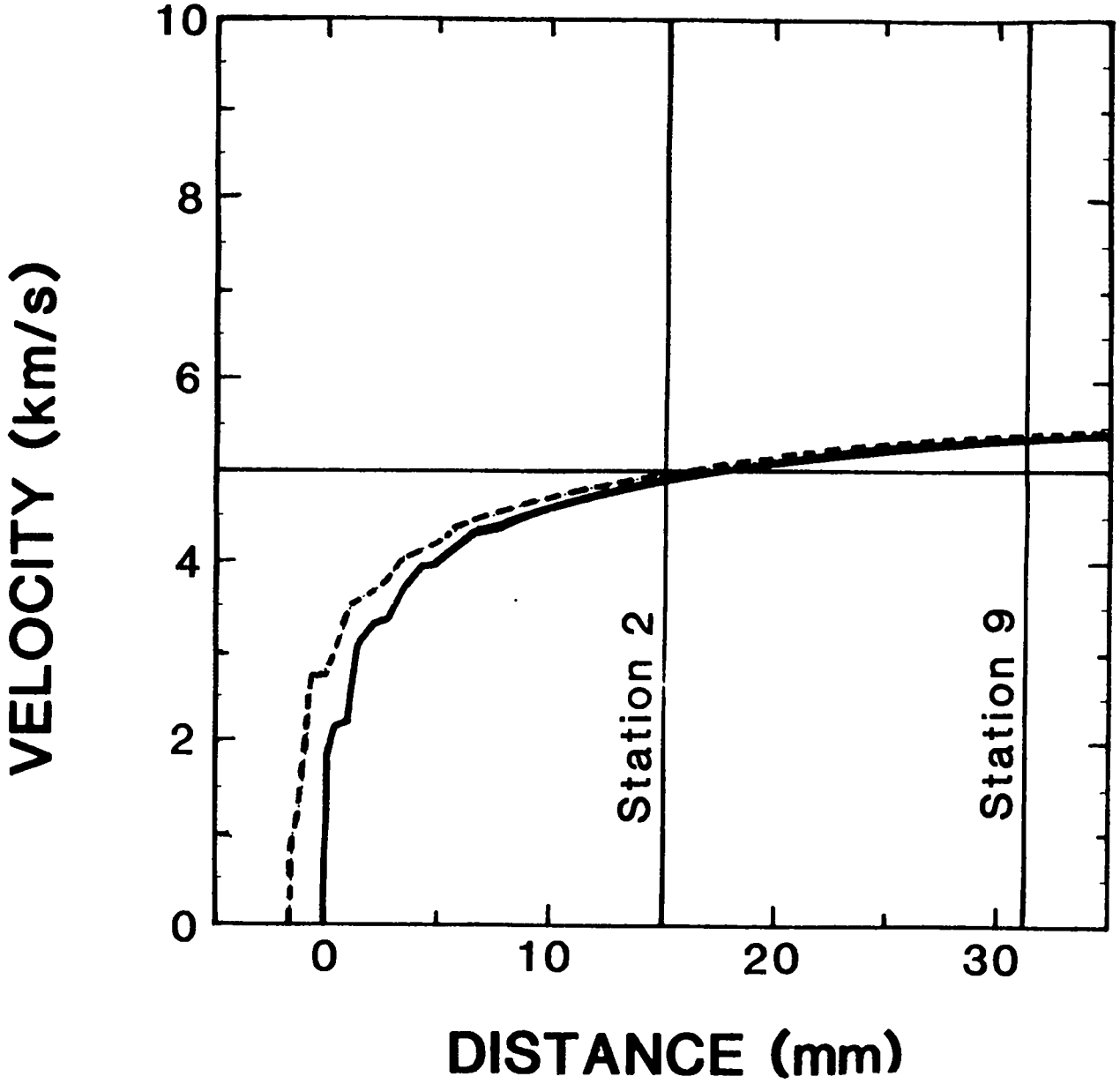

Fig. 17. Calculated velocity of the flyer plate vs distance of run for the front surface (solid line) and back surface (dashed line).

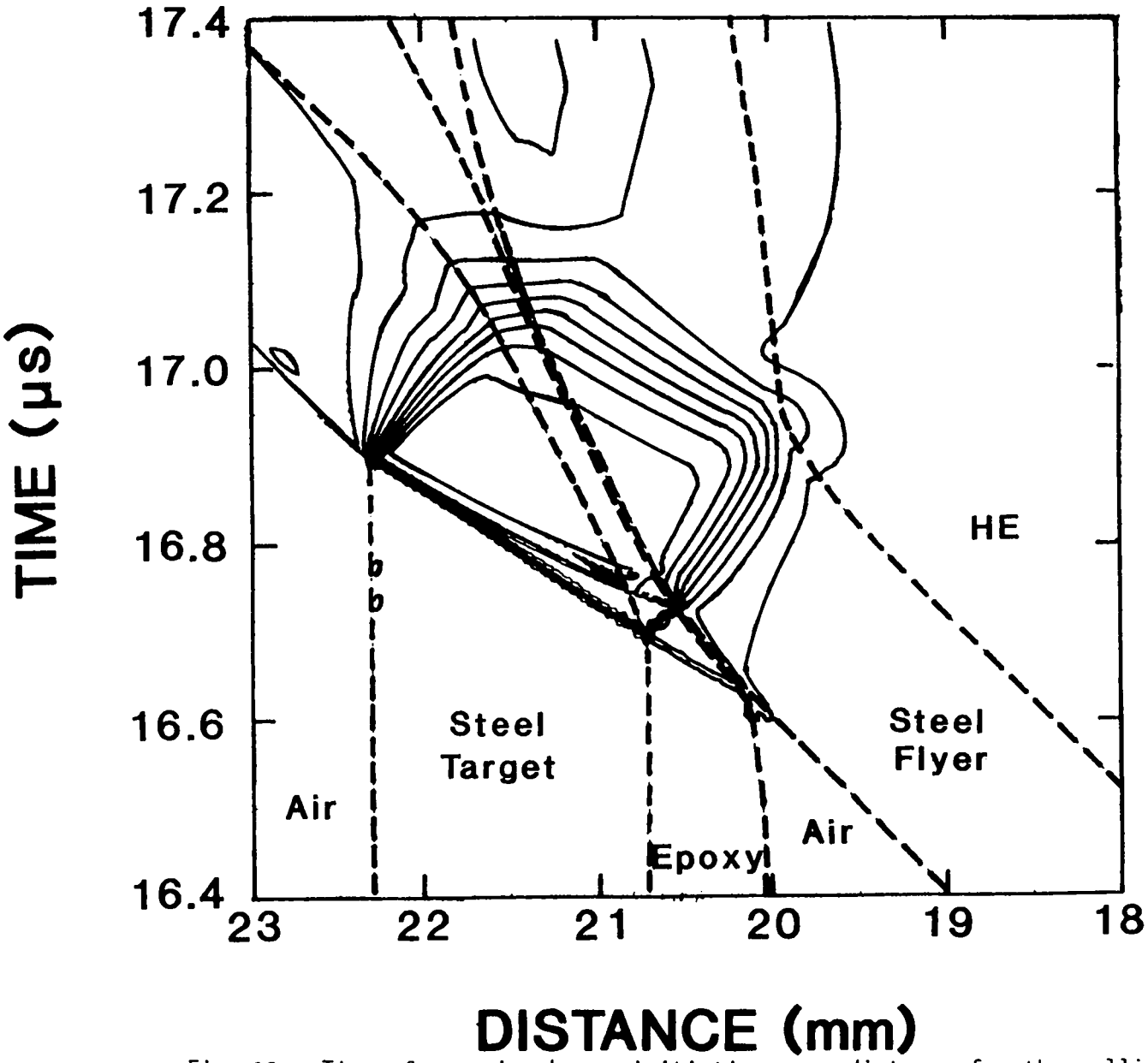

Fig. 18. Time, from main charge initiation, vs distance for the collision between the two steel plates. Trajectories of various interfaces and shock waves are shown. Note that motion progresses from right to left.

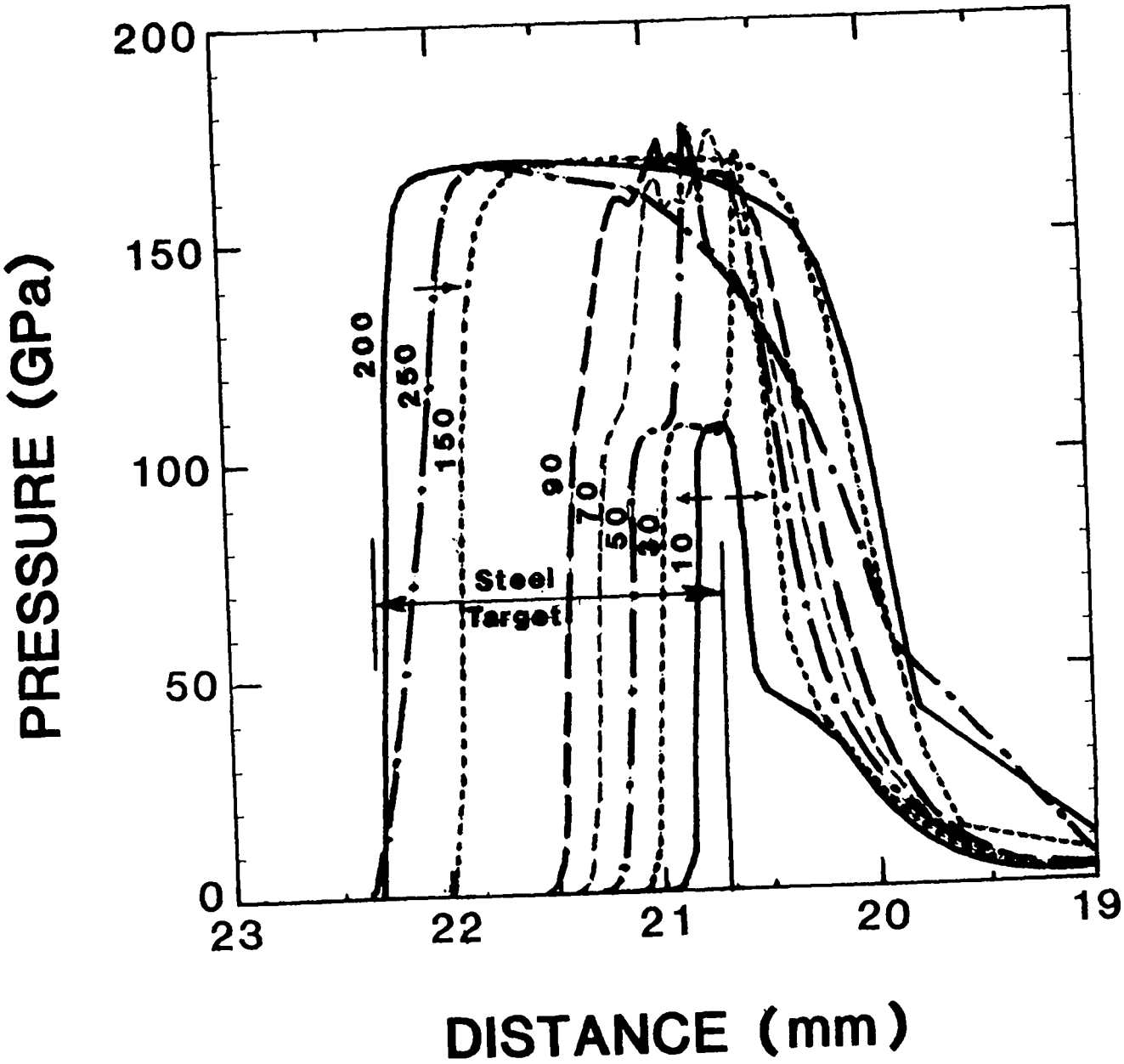

Fig. 19. Pressure profiles in the steel target plate during the collision process. Motion is again from right to left. Profile times are in nanoseconds from first impact on the steel target, or approximately 16.70 μs on the time scale of Fig. 18.

second signal increase vary from 96 to 136 ns, but because of the nature of the shock overtake process, very small experimental irregularities may have a strong effect. The calculated shock velocity in the steel target increases from 7.2 km/s to 8.4 km/s when the reflected shock catches the initial shock.

For the through fibers the first signal comes from the match of the epoxy shock into the quartz. Subsequently, the radial implosion of the fiber by the surrounding shocked steel should strengthen the shock in the fiber and hence increase the light signal. For the surface fibers the light is generated by the quartz shock from the impedance match with the epoxy shock. The pressure in the fiber subsequently rises to that of the impedance match between the epoxy shock and the steel target. The reflected wave in the epoxy, which further raises the pressure, reaches the fiber 0.1 μs later and is too far behind the shock front to affect the light signal.

VII. HYDRODYNAMIC COUPLING OF FIBERS

To use an optic fiber as a pressure transducer, it is necessary to understand the hydrodynamic coupling of the pressure wave in the surrounding material into the fiber. The coupling depends on the geometry and is different for the surface and through fibers. The pressure wave in the surface fiber is driven by the collision of the plate with a velocity vector nearly perpendicular to the fiber axis. Because the phase velocity of the collision is larger than the shock velocity in the fiber, the leading pressure wave in the fiber is an oblique shock. To a good approximation, it may be estimated as a radial shock. Neglecting the curvature of the fiber cross section results in a simple one-dimensional impedance match problem to determine the shock strength in the fiber. Because the detected light is radiated by the leading shock front and the initial shock is oblique, subsequent reflected shocks may be neglected (see Fig. 20).

The pressure wave in the through fiber is driven by a shock in the surrounding medium along the fiber axis. To avoid precursor waves, it is necessary that the shock velocity in the surrounding medium be as large or larger than the shock velocity in the fiber. Due to cylindrical convergence, the shock configuration in the fiber is similar to Mach reflection (see Fig. 21). This is an analogue configuration to the axial shock in a fast shock tube. The incident shock in the fiber may be approximated by a one-dimensional Riemann problem in the radial direction starting with pressure in

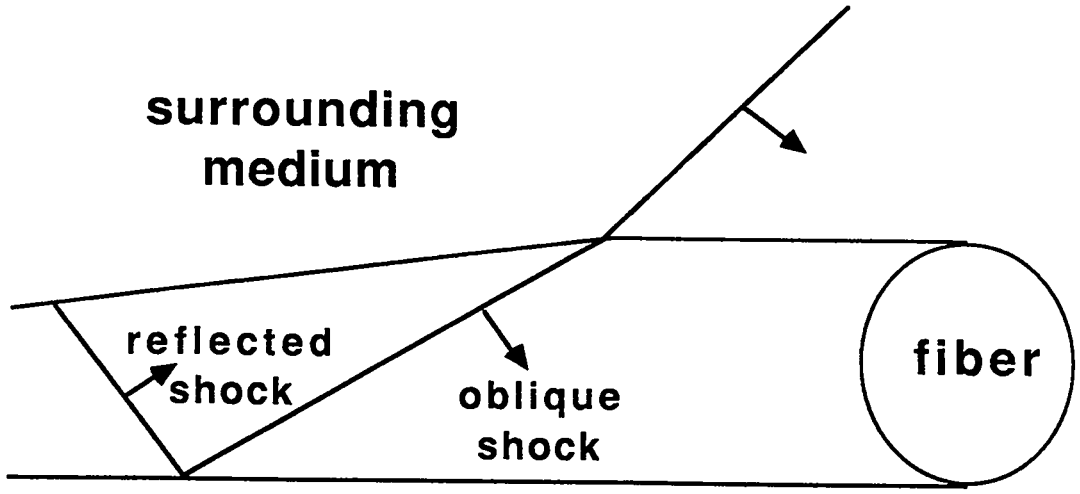

A. Along fiber

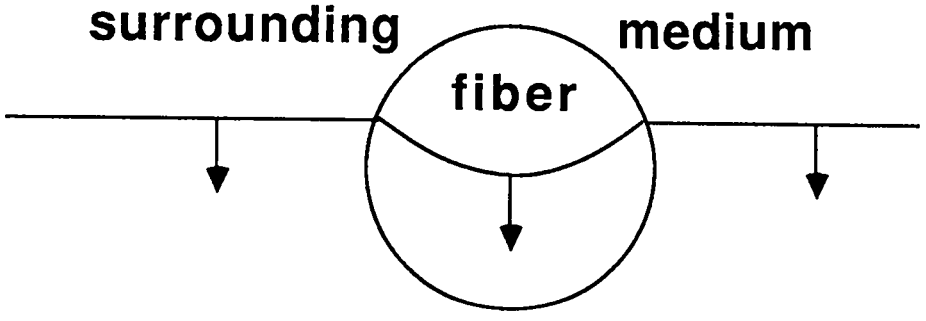

B. Transverse cross section

Fig. 20. Shock configuration for surface fibers.

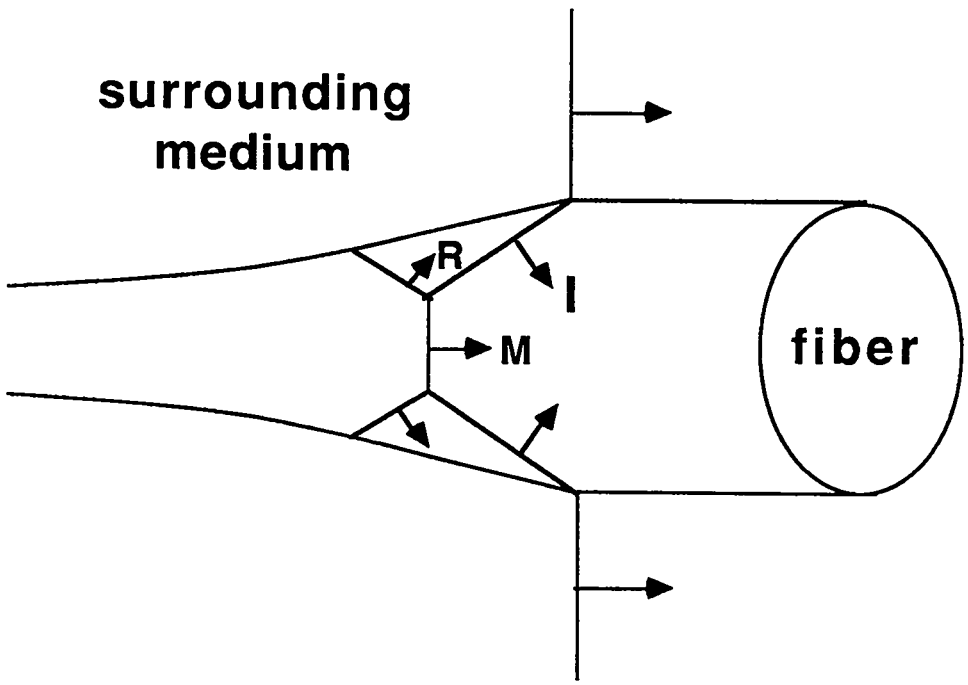

I = incident shock

M = Mach disk

R = reflected shock

Fig. 21. Shock configuration for through fibers.

the surrounding medium but neglecting its axial velocity. The Mach disc in the fiber has the same shock velocity as that of the surrounding medium. The Mach disc is a stronger shock than the incident radial shock and hence, generates more intense light. The complication in computing the total light generated in the fiber is determining the fraction of the cross-sectional area occupied by the Mach disc. Until simple empirical relations are found, two-dimensional hydrodynamic calculations of the fiber in the surrounding medium are needed to relate the measured signal strength from the fiber to the pressure in the medium. Note, the hydrodyamic codes need only an incomplete equation of state, pressure as function of density and specific internal energy, to determine the shock strength. But to determine the light output, the temperature is needed. This makes it necessary to have a complete equation of state parameterization for the fiber (i.e., SiO_2). Also, to avoid precursors (channel shocks), it is important that air gaps between the fiber and surrounding medium be filled with blackened epoxy or the equivalent.

VIII. CONCLUSIONS

Optical fibers can be made to operate as high-pressure shock arrival time detectors, and they give arrival times comparable to or slightly later than those measured with electrical sensors. With optical to electrical conversion, the signals have risetimes that are comparable to those generated with electrical pins. For fiber runs of a few tens of meters, nanosecond precision seems to be possible. Signal-level changes at later times can be interpreted in terms of hydrodynamic events. Calibrated signal levels can be related to temperatures at the shock front in the fiber, which in turn can be related to absolute pressures in the fiber and in the surrounding medium. A number of uncertainties are involved pertaining to the equation of state of quartz and the details of shock impedance matching into the fiber. Nevertheless, satisfactory agreement is obtained between pressures calculated from the fiber signals and those given by the hydrodynamic calculations for the experiment.

ACKNOWLEDGEMENTS

S. A. Colgate, T-6, provided the motivation and theoretical guidance for these experiments. Special mention is given to P. L. Gobby and B. F. Espinoza of MST-7 for assembling the instrumentation on the target plate. J. S. McGurn and B. J. Papatheofanis of P-14 and H. H. Reisch of M-4 arranged the data recording system at the R-306 firing point.

REFERENCES

1. Milton Samuel Shaw and Galen K. Straub, "Hydrox," Los Alamos National Laboratory report LA-8642-M (1981).

2. Gregory A. Lyzenga and Thomas J. Ahrens, Geophysical Research Letters, 7, 141 (1980).

Printed in the United States of America
Available from
National Technical Information Service
US Department of Commerce
5285 Port Royal Road
Springfield, VA 22161

Microfiche (A01)

Page Range	NTIS Price Code	Page Range	NTIS Price Code	Page Range	NTIS Price Code	Page Range	NTIS Price Code
001-025	A02	151-175	A08	301-325	A14	451-475	A20
026-050	A03	176-200	A09	326-350	A15	476-500	A21
051-075	A04	201-225	A10	351-375	A16	501-525	A22
076-100	A05	226-250	A11	376-400	A17	526-550	A23
101-125	A06	251-275	A12	401-425	A18	551-575	A24
126-150	A07	276-300	A13	426-450	A19	576-600	A25
						601-up*	A99

*Contact NTIS for a price quote.

Los Alamos